Single-blind detection, localization, and quantification of methane emissions using continuous path-integrated column measurements

Nathan Blume[1*], Timothy G. Pernini[2], Jeremy T. Dobler[1], T. Scott Zaccheo[2], Doug McGregor[1], Clay Bell[3,4‡]

[1] Spectral Sensor Solutions, LLC, Fort Wayne, IN, USA
[2] Atmospheric and Environmental Research, Lexington, MA, USA
[3] Colorado State University, Fort Collins, Colorado, USA
[4] bpx energy, Denver, Colorado, USA

**Correspondence to*: Nathan Blume (nathan.blume@s-3llc.com)

Abstract

Path-integrated column measurements with a laser absorption-based measurement system have been used to detect, locate, and quantify methane emissions from a series of single-blind controlled releases with no prior knowledge of timing, locations, or release rates. System performance was evaluated against metrics defined in the Continuous Monitoring Protocol established by the Colorado State University Methane Emissions Technology Evaluation Center (METEC). This protocol allows more direct comparison of system performance between disparate measurement technologies and is transferable to any test facility. To the authors' knowledge, this work represents the first time the protocol has been directly applied at a test facility other than METEC. This experiment differs from similar tests where releases were conducted from equipment units at fixed locations at METEC by instead conducting releases at random locations anywhere within the central 0.18 km^2 of a 0.35 km^2 unobstructed test site. The releases were much shorter in duration than those conducted in similar testing at METEC. The system detected 25 of 42 releases with metered rates of 0.17–2.15 kg h^{-1}. The minimum detected emissions rate was 0.22 kg h^{-1}, and the system demonstrated a 100% detection rate for releases ≥0.65 kg h^{-1} and average wind speed <5 m s^{-1}. The test site was subdivided into 20 boxes (109 × 83 m each), and the correct release box was identified in 9 cases, another 9 detections were localized to an adjacent box, and the remaining 7 were attributed elsewhere within the field. The average estimated emission rate bias was −6.1%. The 90% detection limit was 0.89 kg h^{-1}, while the wind-normalized detection limit was 0.44 (kg h^{-1}) (m s^{-1})$^{-1}$.

1 Introduction

Methane (CH_4) is the primary constituent of natural gas, a major source of heating and electricity generation around the world. CH_4 is also a potent greenhouse gas with a global warming potential 81–84 times that of carbon dioxide over a 20-year period (US EPA, 2023; IEA, 2021). The largest industrial sources of CH_4 in the United States are oil and natural gas systems, responsible for an estimated 29% of U.S. CH_4 emissions in 2020 (US EPA, 2022). Accurate characterization of CH_4 emissions in complex environments, such as many oil and gas facilities, is a challenging measurement problem due to limited access, potentially high emission rates creating safety concerns, a large number of potential emission locations, and high temporal variability in emissions (Riddick et al., 2022; Vaughn et al., 2018). In such environments, emissions can occur at many locations and at any time of day and year. Periodic leak detection and repair programs utilizing handheld optical gas imaging sensors, typically performed semi-annually or quarterly, may be effective at finding persistent leaks in expected locations (at equipment prone to leaking or failure), but they do not adequately address the problems of intermittent leaks not emitting at the time

of the leak survey or leaks occurring in unexpected locations that may be omitted from the survey area (Lyon et al., 2015; Nathan et al., 2015; Zavala-Araiza et al., 2015). Periodic airborne leak surveys can have more complete spatial coverage but are generally less sensitive to small leaks, limited to midday periods when the boundary layer is well mixed, and expensive to operate (National Academies, 2018). Furthermore, leaks may persist for weeks or months before being detected by the next periodic survey, potentially resulting in significant total emissions of CH_4 and prohibiting the quantification of such emissions due to the uncertainty in duration. Continuous, wide-area monitoring over entire facilities has the potential to overcome these measurement gaps and to provide rapid detection of leaks with more accurate estimates of total time-integrated gas emissions from oil and gas production, distribution, and storage facilities.

In this single-blind study, a continuous monitoring approach was evaluated based on its ability to detect, locate, and quantify CH_4 emissions with no prior knowledge of emission location, time, rate, or duration. The GreenLITE™ gas concentration measurement system employs continuous laser-absorption-spectroscopy-based, open-path, integrated column measurements in conjunction with a tomographic reconstruction and an inverse dispersion model to locate and estimate CH_4 emission rates. While other open-path continuous monitoring methods require specific knowledge of potential leak locations to pre-position equipment such as reflective targets (Alden et al., 2019), the GreenLITE™ system utilized in this study (consisting of two sensor units) is capable of identifying and localizing emissions from anywhere within the monitoring area. The ability of GreenLITE™ to detect, locate, and quantify CH_4 emissions was evaluated through the use of a set of performance metrics defined in the Continuous Monitoring Protocol (CMP) (Zimmerle, 2020) developed under the Advancing Development of Emissions Detection (CSU, 2022) program run by the Methane Emissions Technology Evaluation Center (METEC) at Colorado State University, Fort Collins, CO. By focusing on top-level metrics such as probability of detection and accuracy of localization and quantification rather than sensor-specific metrics such as sensitivity and signal-to-noise ratio, the CMP aims to provide a means for regulatory agencies and oil and gas operators to directly compare the utility of different monitoring solutions.

Evaluation of other continuous monitoring solutions has been performed at the METEC facility, designed and built specifically for evaluation of CH_4 leak detection and quantification systems. The facility contains decommissioned oil and gas equipment representative of conventional and small non-conventional gas production facilities, namely wellheads, separation equipment, and small liquid storage tank batteries. While METEC provides realistic site topography, experimental design is still critical in evaluating the long-term expected performance of monitoring solutions at operational oil and gas facilities. For example, in prior experiments conducted at METEC in 2018 and described by Alden et al. (2019), for any given test, the pad containing the controlled emission was

known to the sensing system operators, and the sensing system only needed to determine which equipment within the pad the emission source was located on. A total of 17 releases were performed, each lasting 1.5–5.5 hours, with the release beginning and end times known by the sensing system operators. Emission rate and location within the pad were the sole blind aspects of these tests. The experiment provided only a single time window of about 4.25 hours during which no gas was released and false positive (FP) detections were possible. All other results provided were from known controlled releases, limiting assessment of the actual FP detection performance of the system being tested. More recent testing at METEC utilizing the CMP has addressed some of these methodological issues, with participating solutions fully blind, greater numbers of controlled releases, and more continuous operation allowing for greater opportunities for FP detections. (Bell et al., 2023).

The GreenLITE™ experiment detailed here applies the same CMP performance metrics utilized by METEC to a different test site while also attempting to avoid some of the shortcomings of similar monitoring technology evaluations. This study allowed for releases anywhere within 20 grid boxes covering a total area of over 0.18 km^2 at any time within a 12-hour daily window on any of 27 days. The longest release lasted one hour, and the average release was 22.8 minutes in duration. Both point releases and diffuse (area) releases were performed, with diffuse releases occurring at ground level and point releases occurring either at ground level or 1 m above the surface. The GreenLITE™ system operated for more than 314 hours, with releases being conducted during only 5.1% of that time, leaving the rest of that time available for the possibility of FP detections. This experimental design allowed for a more representative assessment of full-time continuous emissions monitoring capabilities over a monitoring area large enough to potentially include multiple operational oil and gas production facilities or represent a much larger single facility such as a refinery or tank farm (Lyon et al., 2016).

2 Materials and methods

2.1 Measurement system

GreenLITE™ is a laser absorption-based gas measurement system that consists of one or more optical transceiver units and some number of retroreflectors arranged such that a clear line of sight exists between each transceiver and each reflector. Backend processing and analytics convert measured optical depth values to dry air volume mixing ratios (henceforth, mixing ratios) in near-real time and generate 2-D distributions of CH_4 mixing ratios (Dobler et al., 2015; Dobler et al., 2017; Zaccheo et al., 2019). GreenLITE™ measurements are interfaced with an inverse dispersion model to estimate CH_4 emission rates and locations. The measurement approach and emission retrieval scheme are described in detail in Pernini et al. (2022).

While GreenLITE™ may be used to measure the mixing ratio over a single atmospheric path, the more common system configuration involves the transceiver scanning to multiple reflectors to measure an area. The transceiver optical head is scanned to sequentially point at each reflector for a period that typically spans 10–30 seconds depending on the application, measuring the path-integrated mixing ratio of the target gas along the straight-line path ("chord") from the transceiver to the reflector. If two transceivers are arranged such that their measurement chords intersect one another (as seen in Figure 1, for example), a 2-D reconstruction of the distribution of the gas mixing ratio over an area that can span up to 25 km^2 can be obtained using a sparse tomographic approach (Dobler et al., 2015; Dobler et al., 2017).

Prior to this experiment, GreenLITE™ has previously been tested and deployed in several environments for CO_2 and CH_4 monitoring, including a 6-month study to monitor for CO_2 leaks from an underground carbon storage facility (Blakley et al., 2020), a 1-year study to monitor urban CO_2 emissions over central Paris, France (Dobler et al., 2017; Zaccheo et al., 2019; Lian et al., 2019), a 1-week evaluation of the CH_4 and CO_2 leak quantification ability of GreenLITE™ at an oil and gas facility (Watremez et al., 2018), and multiple campaigns monitoring fugitive CH_4 and CO_2 emissions from an oil sands open-pit mine and tailings pond (Pernini et al., 2022).

2.2 Measurement site

The experiment detailed in this paper was designed to simulate the area of a typical oil and gas storage tank farm. The chosen test site was a farm located in a rural area at the edge of a more suburban area. The site was mostly flat with few obstructions. While no known sources of CH_4 were present in the immediate vicinity of the test site, highways, shopping centers, housing developments, railroad tracks, and several active farms were present within a 2-km radius. While testing at a known experimental site such as METEC was considered, a site near the GreenLITE™ manufacturer was selected for these first blind tests based on experimental design consideration and time/cost constraints. Though the METEC facility more realistically represents infrastructure at a typical oil and gas facility, GreenLITE™ is well suited for monitoring areas much larger than the approximately 0.03 km^2 METEC site. A GreenLITE™ deployment could monitor an area large enough to include multiple oil and gas production sites or a much larger single facility such as a refinery or tank farm. Furthermore, longer path lengths benefit the GreenLITE™ differential absorption measurement via higher signal-to-noise ratio due to the chosen wavelengths. The selected test site and methodology were reviewed by a METEC representative involved in the development of the CMP. By performing the experiment on a much larger scale than what is possible at METEC, this work demonstrates that the CMP is transferrable to any potential test location, enabling adaptation for a wider range of

developing technologies. To the authors' knowledge, prior to this work, the CMP has not been applied to controlled release testing anywhere outside the METEC facility.

Detection, quantification, and localization performance metrics for the GreenLITE™ system (or any continuous monitoring sensor) may be expected to vary in different environments due to differences in area, topography, meteorology, and on-ground infrastructure, and the authors acknowledge that results from similar testing performed at an operational oil and gas facility would likely differ from the results of this work. Specifically, the lack of oil and gas equipment on the test site used for this work significantly reduces the turbulent mixing that occurs in the presence of such equipment. The GreenLITE™ emissions measurement approach is robust in that measurement lines of sight and heights can be readily adapted to a given site by optimizing transceiver and reflector locations and heights for the site-specific application.

Meteorological data were provided by an onsite ATMOS 14 (measuring temperature, pressure, and relative humidity) and an ATMOS 22 (measuring wind speed and direction) from METER Group. See Appendix A for a more detailed description of the meteorological conditions experienced during testing.

2.3 System installation and setup

GreenLITE™ was set up at the farm test site as shown in Figure 1. The layout included two GreenLITE™ transceivers and 29 retroreflectors arranged to provide 54 measurement chords covering an area of 0.35 km^2. Because of the flat site topography and lack of obstructions, all chord endpoints (transceiver optical heads and retroreflectors) were simply placed two meters above ground level, with optical heads mounted on custom pipe-frame structures and retroreflectors mounted on tripods. Chords measured 216–817 m in length. The measurement area was subdivided into 44 potential emission location boxes. Releases could be conducted in any location other than the outermost boxes (for a total of 20 potential release boxes equaling 0.18 km^2). The buffer boxes around the perimeter ensure that emissions within the site are not missed regardless of wind direction. While GreenLITE™ is able to monitor much larger areas (Dobler et al. 2017; Pernini et al., 2022), the area monitored in this experiment was primarily limited by property lines. Testing was performed in the time period from January to April, 2022, over a range of weather conditions. Local meteorological data were provided by an onsite weather station installed near transceiver T01 (green marker near lower left of Figure 1).

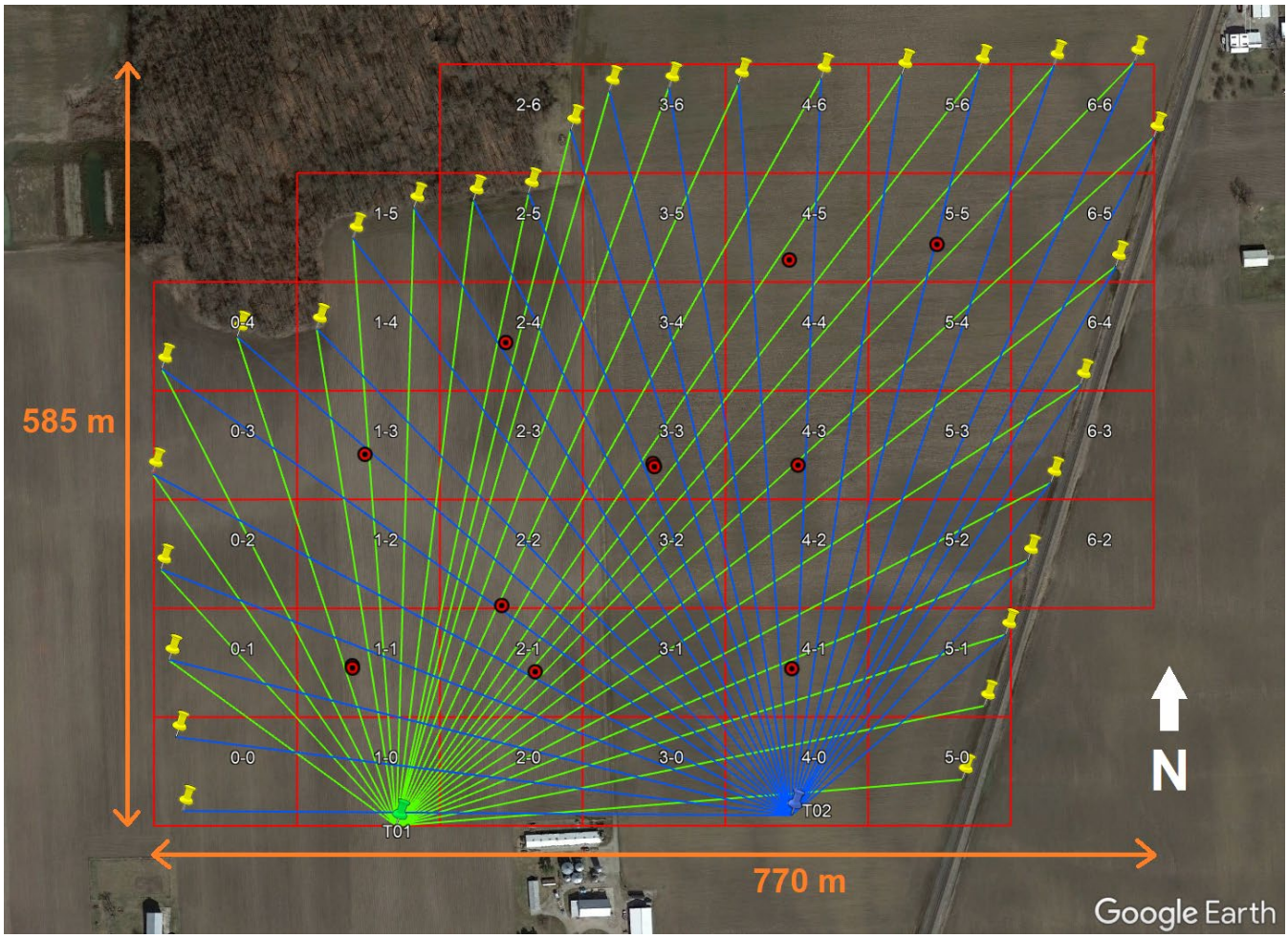

Figure 1. Layout of GreenLITE™ system at the test site. T01 and T02 are the two transceiver locations along the southern edge, yellow markers are the reflector locations, green lines are the chords measured by T01, and blue lines are the chords measured by T02. The red boxes are used as bounding boxes for computing emissions and providing an estimated location of the emission. Blind controlled release locations are marked with red and black bullseye symbols. Map Source: Google Earth © 2020

The system was installed in a non-permanent manner to avoid disruption to ongoing farming activities. Consequently, frequent ground freeze-thaw cycles experienced throughout the winter-spring testing period impacted optical alignment between the transceivers and reflectors. This was expected but unavoidable given the installation constraints. While GreenLITE™ is tolerant of very minor disturbances in optical alignment, larger disturbances result in the transmitted laser missing the reflector and causing insufficient optical power to be collected by the transceiver. Regular realignment was performed via the system's remote interface on all testing days, including both days when releases were performed and days when no releases were performed. Realignment

entailed making minor adjustments to the programmed scanner positions that are used to point the sensor optical head at each of the reflectors to compensate for the platform movement. Such realignment is not needed when GreenLITE™ is installed in a semi-permanent or permanent fashion, as was done in the deployments described by Dobler et al. (2017), Pernini et al. (2022) and Blakley et al. (2020).

2.4 Unblind release testing

A set of unblind releases was conducted in mid-January to evaluate the release procedure and verify expected performance. High-purity gas consisting of 99–99.5% pure CH_4 was used for all releases. Appendix B contains more information about the release system. A second round of unblind releases was conducted in late-January, allowing the detection sensitivity of the system to be coarsely evaluated and adjusted while providing guidance regarding the range of release rates that would be appropriate for the ensuing blind release tests. These unblind releases were performed at rates of 0.17–2.15 kg h^{-1}. While storage tanks are known to be frequent emitters of CH_4 (Lyon et al., 2016), very little literature exists regarding true leak emission rates from oil and gas storage tanks due to the challenges associated with direct measurement of such leaks (Johnson et al., 2022). The release rates tested in this experiment are expected to be smaller than true emission rates from storage tanks and serve as an evaluation of the lower detection thresholds for the GreenLITE™ system. In theory, no upper detection limit exists for GreenLITE™, but quantification performance at higher emission rates may differ from that at the lower rates tested in this work.

Prior to conducting any blind releases, the test plan and test setup were audited onsite by a representative from METEC, whose recommendations were incorporated into the final test and execution.

2.5 Blind release testing

Recent evaluation of continuous monitoring systems at METEC included hundreds of individual releases, some lasting up to 8 hours, at emission rates up to 6.39 kg h^{-1} (Bell et al., 2023). In this study, releases were limited to rates ≤ 2.15 kg h^{-1} and durations ≤ 60 minutes due to limitations of the release system hardware and the prohibitive cost of large quantities of methane gas. Initial unblind test results indicated that high release rates were not needed to identify the minimum detection threshold and that short durations would provide ample information on detection thresholds to determine the 90% probability of detection emission rate. Blind releases ranged in duration from 12 minutes to one hour, with the average release lasting 22.8 minutes.

Personnel involved in this experiment were split into two groups: the test center team, responsible for planning, executing, and documenting the controlled releases; and the performer team, responsible for maintaining system

operation and identifying, locating, quantifying, and reporting emission events. The test center team provided no information to the performer team regarding test days, times, durations, locations, or emission rates. This arrangement ensured that the performer team remained fully blind to the release schedule and details to allow for an unbiased assessment of the emission detection, localization, and quantification capabilities of GreenLITE™. For each release event, the test center team recorded all relevant information about the release. Releases occurred on six separate days dispersed over a six-week period containing 27 potential release days – 30 weekdays minus two days for power outage and one day for equipment maintenance. All releases occurred between 8:00 AM and 6:00 PM local time to ensure system alignment and to minimize the impact of frost heaving. Releases were conducted at 10 unique locations indicated in Figure 1, with releases being repeated at two of those locations on different days.

A histogram of the releases as a function of release rate is provided in Figure 2 (left). The right plot of Figure 2 shows the number of GreenLITE™ scans as a function of release rate, which considers the duration of the release and the instrument scan rate. A complete scan producing mixing ratio measurements on all 54 chords took approximately four minutes. More releases were performed at lower emission rates to improve confidence in the probability of detection evaluated at those rates, and higher emission rates were conducted for shorter release periods to limit gas consumption.

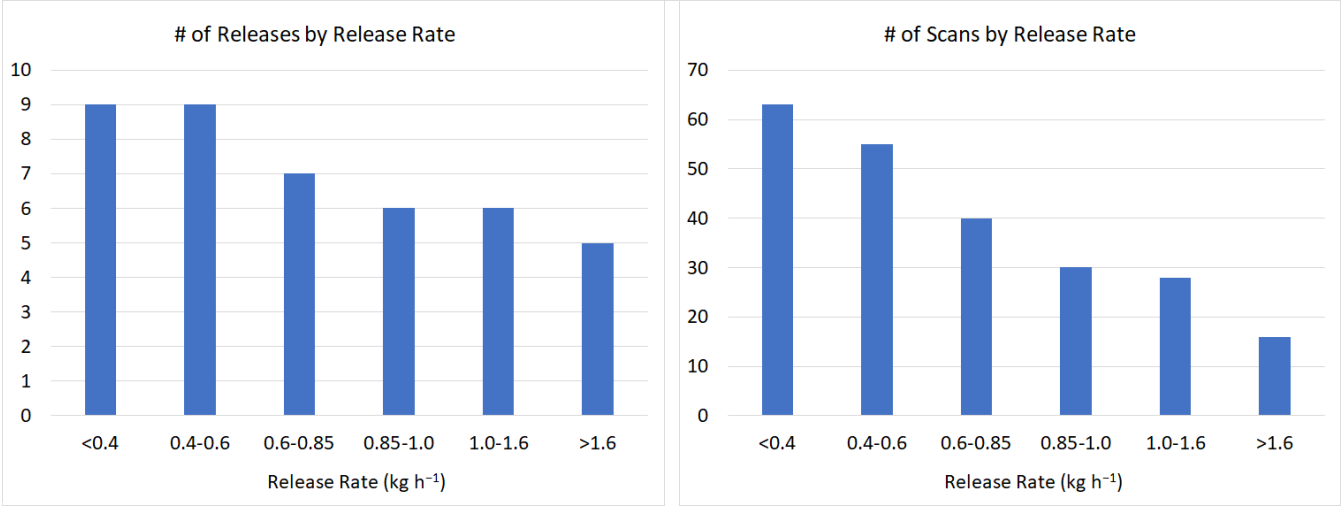

Figure 2. Distribution of releases and system scans as a function of release rate. Distribution of the 42 releases as a function of release rate (left); Distribution of 4-minute GreenLITE™ scans of the monitored area as a function of release rate (accounts for release duration at each rate) (right).

If any emission events were detected, emission rates and locations were estimated for each detection or group of detections. All detections, localization and quantitative estimates were computed by the single-blind performer team at that time and reported for comparison to the test center team release record upon completion of blind testing.

2.6 Detection of emission events

The chord mixing ratio measurements were passed through a detection algorithm to identify likely emission events. The median of all chord mixing ratio measurements over a rolling time window was used to correct for natural variations in atmospheric background CH_4 mixing ratio. Median chord-to-chord differences were removed through a flat-fielding correction prior to identification of chord mixing ratio measurements exceeding the detection threshold. For each detection, the sample time, chord ID, and measured chord mixing ratio were recorded in the detections file for that day.

2.7 Emission localization and quantification

The integrated column mixing ratio measurements were combined with local wind information to create 2-D estimates of mixing ratios within the plane defined by the chords and their intersecting horizontal area using a sparse tomographic approach that minimizes the error between an analytical model of the field and the observed chord mixing ratio values (Pernini et al., 2022). The 2-D mixing ratio field is modelled as a set of rectangular subregions ("boxes").

The approach adopted in this study was to combine box retrieval data with a standard emissions modelling framework called Second-order Closure Integrated puff model with Chemistry (SCICHEM) (Chowdhury et al., 2015). In this application, SCICHEM is used in an iterative scheme to provide emission estimates in the box sectors depicted with red lines in Figure 1.

Detection times were used to determine which time periods to process for emissions estimation. Emission rates and locations were computed for each 10-minute time period in which an emission event had been identified by the detection algorithm. Since the mixing ratio values associated with the 2-D box reconstructions are used in the iterative inverse dispersion model emission retrieval scheme, emission locations were estimated to the fidelity of the red boxes shown in Figure 1, with each emission event assigned to a numbered box. Emissions for each reconstruction box were computed, and the largest emission value in a non-edge box was provided as the estimated emission rate and the box as the emission location. The estimated emissions results, including the time window, emission rate, emission location, and average wind speed and direction over the time window, were recorded in the

emissions file for that day. Emission rates were estimated in units of grams per hour (g h^{-1}) as per the CMP, but results are presented here in kg h^{-1}.

3 Results and discussion

Upon completion of all controlled releases, the reported detections and emissions results were compiled and compared to the test center release log data. Performance metrics were computed as defined in the CMP. Full results from each blind controlled release are provided in Appendix C.

3.1 Detection results

The primary CMP metrics related to detection are Probability of Detection (PD), False Positive Fraction (FPF), False Negative Fraction (FNF), and Detection Time. PD is simply the number of true positive (TP) detections divided by the sum of the number of true positive and false negative (FN) detections. PD represents the fraction of emission events that were correctly identified.

The distribution of releases and detection as a function of release rate is shown in Figure 3. A logistic regression is used to create a smooth, continuous PD curve from the discrete data samples, while a bootstrapping technique provides an indication of uncertainty in the result if experiments were repeated. Figure 4 shows bootstrapped logistic-regression PD curves based on all detections from each release. This approach considers the number of releases at a given rate and the length of the releases. The bootstrapping technique envelopes the expected detection performance of the system under test and is performed by randomly selecting N detection samples out of N actual detections (with replacement) prior to performing the logistical regression. This process is repeated 100 times to build the grey curves seen in the left panel of Figure 4, and the blue curve is the logistic regression fit to the estimated emissions.

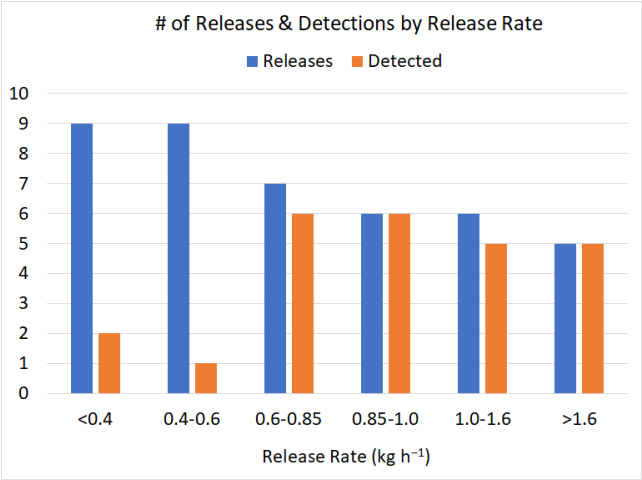

Figure 3. Distribution of releases as a function of release rate. All releases are shown in blue, while only those released that were detected are shown in orange.

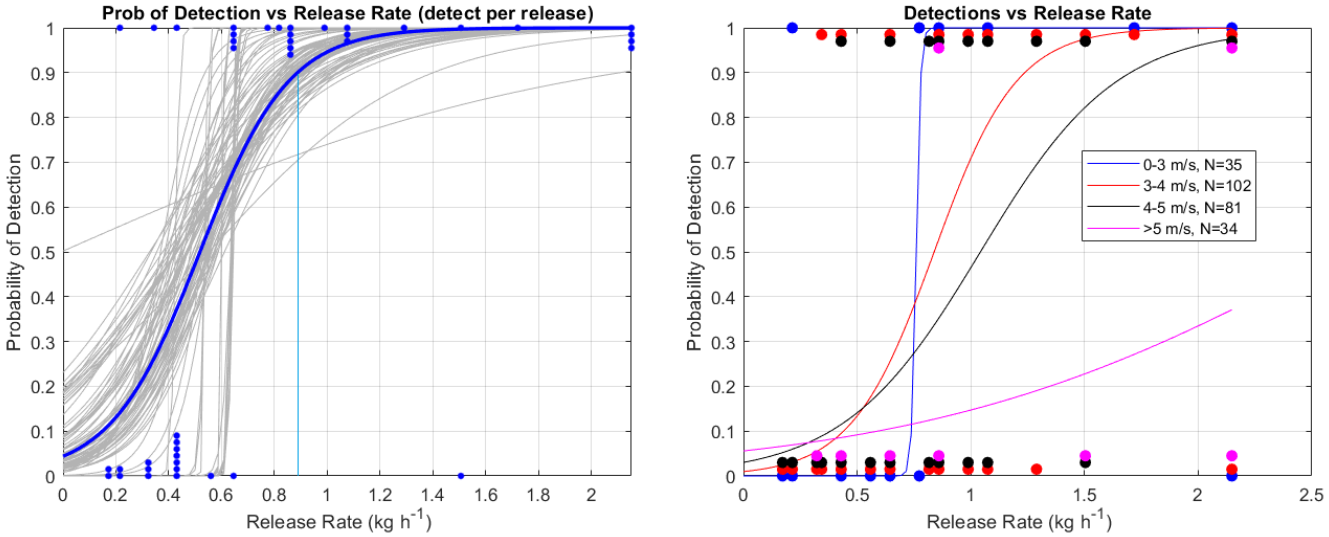

Figure 4. Probability-of-detection curves as a function of release rate. Probability of detection (blue: fit to data, grey: bootstrapping iterations) as a function of release rate (left); Probability of detection versus release rate and binned by wind speed (right). The left plot shows a 90% detection limit of 0.89 kg h^{-1}. Filled circles represent individual samples (detection or non-detection) and are stacked to show the number of samples at a given release rate.

The right panel of Figure 4 shows the PD curves, binned by average wind speed during the release, using a logistic regression without bootstrapping of the data. Note that the binning was chosen due to the limited number of samples at lower and higher wind speeds. The right panel of Figure 4 indicates that one of the primary drivers of uncertainty in the PD curve is wind speed. To evaluate this further, a logistic regression with bootstrapping was performed

using the release rate normalized by wind speed, consistent with analysis by Bell et al. (2022) and Sherwin et al. (2021) in the evaluation of other remote sensing systems. The result is illustrated in Figure 5 and shows a narrower confidence interval seen as a tighter grouping of the 100 bootstrap results.

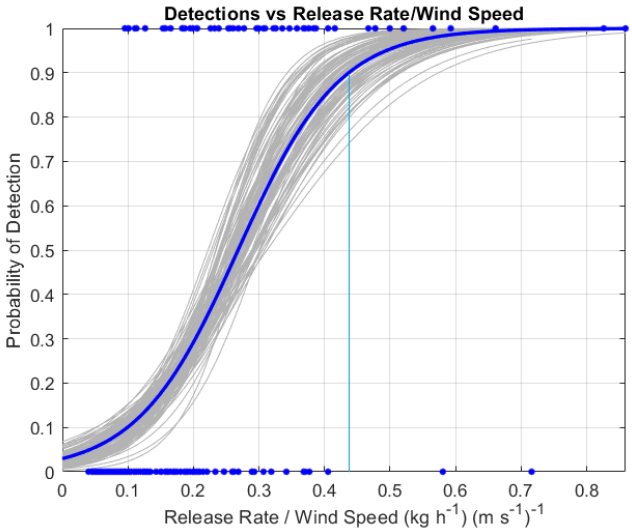

Figure 5. Logistic regression with bootstrapping using release rate normalized by wind speed. Normalization of release rate by wind speed shows a 90% detection limit of 0.44 (kg h^{-1}) (m s^{-1})$^{-1}$. Filled circles represent individual samples (detection or non-detection).

Not captured in the previous figures is the number of FP detections and the FPF. FPF is the number of FP detections divided by the total number of reported detections. By definition, a FP detection is a reported detection that occurred at a time when no controlled release was being conducted. However, due to the uncontrolled nature of the test site and the fact that it is surrounded by a variety of potential CH_4 sources (e.g., homes, farms, forest, roads and highways, railroad tracks, shopping centers), a reported detection outside of a controlled release time may in fact be a detection of a true elevated CH_4 mixing ratio from a source outside the monitored area. The CMP instructs that detections classified as originating from outside the facility are to be omitted from the classification process and calculation of FPF. Appendix D contains details about two days on which off-site emissions sources were observed.

The total number of reported FP detections during the 6-week testing period was 31. These 31 FP detections occurred during a total non-release monitoring time of 298 hours and 17 minutes. The breakdown of FP detections between days with and without controlled releases (Table 1) shows no significant difference in FP rate between release and non-release days.

Table 1. Breakdown of FP detection frequency on days with and without controlled releases

Classification	# Days	# FP Detections	FP/Day
Days with Release	6	8	1.33
Days without Release	21	23	1.10

The CMP defines FPF as the number of FP detections divided by the total number of reported detections (FP + TP). The drawback to this definition is that the FPF is influenced as much by the number of releases and resulting TP detections as it is by the number of FP detections. A test consisting of many controlled releases and a short time period in which no releases are conducted will result in a lower FPF than one in which only a few releases are performed over a long period of operational time (as in the case of this experiment).

As defined by the CMP, the GreenLITE™ FPF for this single-blind test was 0.261 (31 FP of 119 total reported detections). Computing FPF in a manner similar to how FNF is computed may be more meaningful. FNF is defined as the number of FN detections divided by the number of controlled releases, which represents the fraction of controlled release periods not containing at least one TP detection. Alternatively, dividing the number of FP detections by the number of non-release periods represents the fraction of non-release periods containing at least one FP detection. We define this alternative metric as FPF′. A non-release period is defined as a period of time equal to the average duration of all controlled releases but containing no controlled release.

The average release duration for this experiment was 22.8 minutes. The total non-release time divided by the average release period yields 785 time periods of 22.8 minutes during which no controlled releases were conducted and results in a FPF′ of 0.039.

The FNF for this experiment is 0.40 for all release rates. Note that the FNF is influenced by the distribution of emission rates included in the experiments and is therefore more meaningful when considered as a function of release rate, as shown in Figure 6. With the objective being to characterize the low-end sensitivity of the GreenLITE™ system, the vast majority of releases that did not produce detections were at relatively low rates (< 0.65 kg/h). The single FN detection at a rate greater than 0.65 kg h^{-1} (see Figure 3) was associated with a 16.7-minute release at 1.51 kg h^{-1} during which the average wind speed was 5.6 m s^{-1} (the highest of all controlled releases).

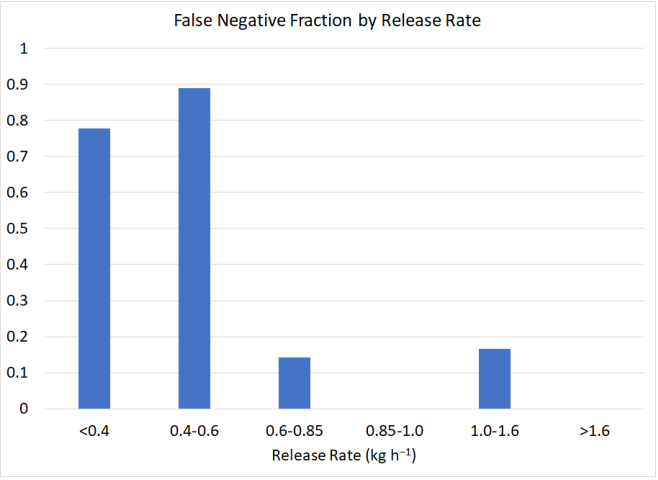

Figure 6. False negative fraction as a function of release rate. With the exception of a single false negative detection at 1.51 kg h^{-1}, the false negative fraction distribution shows a steep decrease above 0.6 kg h^{-1}.

Detection Time is defined as the elapsed time between the start of a release and the time when the release is first reported. Detection Time values in this experiment ranged from 46 seconds to just under 23 minutes and exhibited an inverse relationship with metered release rate. Detailed Detection Time results are given in Appendix E.

3.2 Emissions localization results

The primary metrics related to emission localization defined by the CMP are Localization Precision and Localization Accuracy. The CMP requires that a detection report specify the emission location by identifying the Equipment Unit ID to which the emission is attributed. If an emission is believed to have originated from outside the testing area, it may be classified as Off Facility and excluded from the calculation of metrics. Because this experiment was performed in an agricultural setting and not on an operational or simulated oil and gas production facility, the test site included no equipment to which emissions could be attributed. Instead, each grid box (see Figure 1) was assigned a unique Cell Unit identifier to which an emission event believed to have originated from within that area could be attributed to. The boxes immediately adjacent to a given box were defined as the Cell Group. Each detected emission location was reported to the Cell Unit level (i.e., to a specific box), and the reported locations were then compared to the true locations to compute the localization precision and accuracy metrics.

Localization Precision is simply a count of the number of detected releases that were identified to the correct Cell Unit, Cell Group, and Facility levels. Of the 25 detected blind controlled releases, 9 were correctly localized to the Cell Unit level (box), 9 others to the Cell Group level (adjacent box), and the remaining 7 to the Facility level (elsewhere within measurement footprint). A subset of the Cell Group level detections included true release

locations that were near the box boundary of the nearest downwind neighboring box. For these releases, wind likely carried the gas plume to a downwind measurement chord that passed through the neighboring box which was subsequently estimated to be the release box. In future work, both the proximity of the chord for which a detection occurred to respective box boundaries as well as wind speed/direction will be accounted for when localizing leaks, which should improve localization accuracy.

The Localization Accuracy metric represents the fraction of all detections (both TP and FP) that were correctly identified at the Unit, Group, and Facility levels of precision. A detection correctly localized to the Unit level also counts as a detection at the correct Group and Facility levels. The GreenLITE™ Localization Accuracy metrics were also calculated with FP detections omitted from the denominator, as was done by Bell et al. (2023), since the number of FP detections is a function of total monitoring time rather than the number of releases. The Localization Accuracy results are presented in Table 2.

Table 2. Localization Accuracy metrics as defined by the CMP and with FP detections omitted

Localization Accuracy Definition	Cell Unit	Cell Group	Facility
As Defined by CMP	0.161	0.321	0.446
With FP Detections Omitted	0.360	0.720	1.000

3.3 Emissions Rate Quantification Results

A secondary metric of the CMP is emission rate quantification accuracy. Emission rate quantification accuracy typically benefits from the averaging that longer release durations permit, whereas the short releases executed in this experiment presented a highly challenging scenario with little to no opportunity to average emissions estimates. The overall results of estimated emissions versus metered rates are provided in Figure 7. The figure depicts the linear fit between the estimated and metered emission rates for all releases. Horizontal error bars represent the standard deviation of the metered release rate as measured throughout each release. These results indicate a bias of -6.1% from the linear fit with a fixed zero intercept. Relatively high variability is seen for release rates that were repeated multiple times, which may be due to a number of factors including wind conditions and proximity of release location to the nearest downwind measurement chord. Quantification error of individual rate estimates ranges from −89% to +263% of the metered release rate, with 80% of estimation errors falling between −67% and +67%.

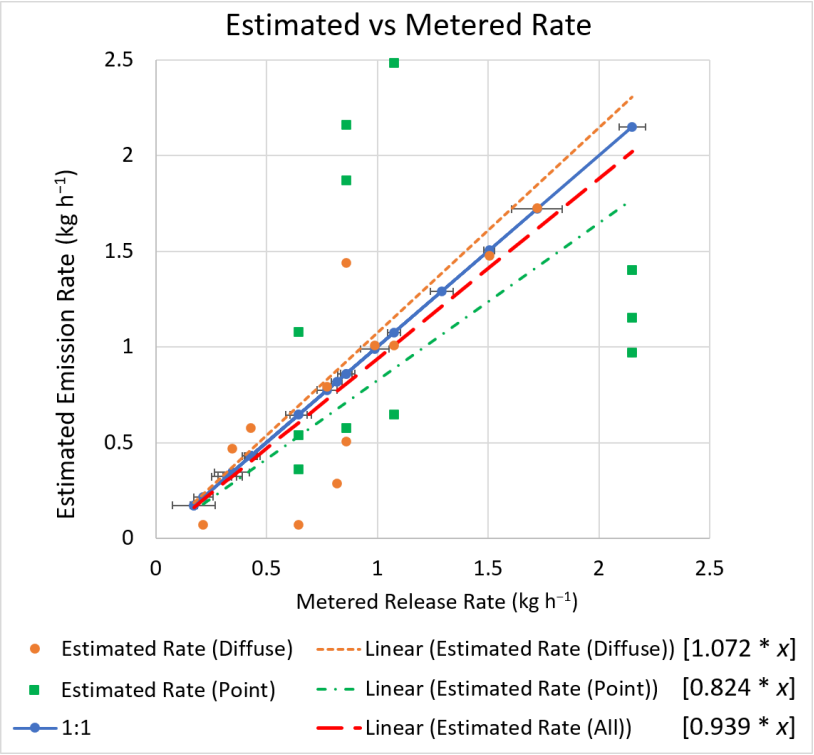

Figure 7. Estimated emission vs. metered release rates for all detections, separated by release method. Point releases are depicted with green squares, and diffuse releases are shown as orange circles. This plot illustrates the fit relationships between metered and estimated rates for the entire set of detections achieved during this testing as well as for the detections separated by release method. Linear fits with no intercept indicate bias of +7.2% and −17.6% for diffuse (orange dotted line) and point (green dashed-dotted line) releases, respectively, while the fit to the entire dataset indicates a bias of −6.1% (red dashed line).

The quantification results presented here are representative only of the limited range of emission rates included in this experiment, which were selected to develop confidence in the PD curve as opposed to confidence in the quantification estimates over a much broader operational range. Quantification performance may be better or worse at higher emission rates, and further testing is required to determine the quantification accuracy of GreenLITE™ for larger emission events. Also of note is the apparent difference in quantification accuracy between point and diffuse releases, with some of the point release estimates falling further from the linear fit line than all of the diffuse release estimates.

3.4 Operational factor

The last primary metric defined by the CMP is Operational Factor, which represents the fraction of time a system is operational relative to the total planned testing time. The total planned testing time was 345.4 hours, while the

operational time totaled 314.2 hours, for an Operational Factor of 0.910. Causes of down time included laser beam attenuation due to thick fog and heavy rain, failure of a component power supply, and operator error. This calculation does not include the two periods of time when power to the equipment was disrupted due to a local power outage.

4 Conclusions

4.1 Results summary and implications

The results from this single-blind study show that, with no prior knowledge of potential leak locations, rates, times, or durations, GreenLITE™ can detect CH_4 emissions as small as 0.22 kg h^{-1} and that, for the 22 controlled releases with average wind speeds <5 m s^{-1}, it demonstrated a 100% detection rate for leaks ≥ 0.65 kg h^{-1}. Of the 42 releases in total, 25 were detected as emission events. For localization, the correct release box (Unit) was determined for 9 of the detections, an adjacent box (Group) was identified in 9 of the detections, and the remaining 7 were localized elsewhere within the field (Facility). Quantification of the 25 detected emissions exhibited a bias of −6.1%. Prior work (Pernini et al., 2022) demonstrated that primary sources of uncertainty in emission rate estimates are variability in averaged surface meteorology and surface meteorology measurement precision, while chord concentration measurement accuracy and error in dispersion modeling are not significant contributors to uncertainty (estimated to be less than 5%). These results represent an important first step in demonstrating feasibility of the GreenLITE™ system to offer continuous monitoring of relatively large oil and gas facilities to identify, locate, and quantify CH_4 emission sources, including those from arbitrary locations at random times.

Additional testing to further assess the capabilities of GreenLITE™ for use in monitoring oil and gas facilities should include the presence of multiple emissions sources, allowed (known or expected) emission events, and higher emissions rates, as well as testing in a more relevant environment containing oil and gas equipment and infrastructure.

While the CMP metrics are a useful framework for providing a method to compare the key characteristics of continuous monitoring systems that are most of interest to oil and gas operators and regulators, our work illuminates some refinements that could be made to further increase the utility of the metrics. Limitations of the CMP methodology to perform classification of detections as TP or FP detections have been identified in other testing programs (Bell et al., 2023), suggesting a need to consider the application or use case of the continuous monitoring system under evaluation and to tailor the methodology as appropriate. Defining FPF such that it is not dependent on the number of controlled releases would allow more meaningful comparison between systems tested under very

different experimental designs. One such solution would be to compute FPF as the number of FP detections reported per 24-hour period of system operation. A modified Localization Accuracy metric that does not utilize the Unit/Group/Facility classification method would provide more consistency across monitoring systems intended for different use cases. The experiment detailed here was intended to evaluate the ability of GreenLITE™ to detect, quantify, and localize leaks from oil and gas storage tanks rather than from well pads. Thus, an equipment Unit was defined to be much larger in size than it would have been if attempting to localize a leak to a specific valve or compressor. Determination of Localization Accuracy using some distance-based measure would allow better comparison of results from testing performed at facilities of different scales.

4.2 Potential future improvements

The GreenLITE™ emission detection algorithm can be modified to apply a temporal requirement such that multiple detection events must occur within a specified time window before a detection is reported. This change will result in a reduction in FP detections and increase confidence that reported detections are TP detections. Due to the relatively short duration of releases included in this experiment, a quantitative analysis of the potential improvement was not conducted.

Emissions localization and quantification may be improved by more fully utilizing measured wind speed and direction as well as the proximity of measurement chords to box boundaries. For example, a localization constraint limiting possible predicted leak locations to boxes that fall on or upwind of detection chords may further improve localization performance. Emission localization and quantification accuracy may also be improved by using a Gaussian plume reconstruction approach with the emission source modeled as a point emission in the inverse dispersion model rather than the box reconstruction with area emission sources. This is supported by the quantification estimates separated by release type, shown in Figure 7, which show better agreement between estimated rates for diffuse releases than for point releases using the box reconstructions.

Appendix A: Test conditions

Average temperatures during the test period ranged from −6° C in Jan/Feb to +15° C in April. Average wind speed for the test period was 3.2 m s^{-1}, with the prevailing wind out of the southwest and west, as shown in Figure A1.

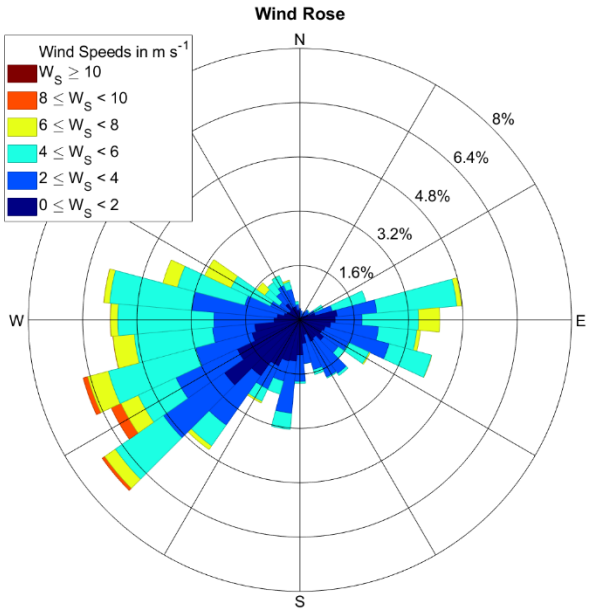

Figure A1. Wind rose depicting distribution of wind direction and speed during blind testing period. During the blind testing period of 15 Mar–26 Apr, 2022, the wind was predominantly from the West to Southwest.

Appendix B: Controlled release system

The controlled release system consisted of a pressurized cylinder containing of 99–99.5% pure CH_4, a single-stage regulator, an Omega FMA-1609A mass flow meter (2.15 kg h^{-1} max), a computer with custom software for logging the flow meter output, a 15-meter vinyl hose, and a 3 m × 3 m PVC pipe diffuser (optionally attached for "diffuse source" releases). A diagram of the release system is shown in Figure B1.

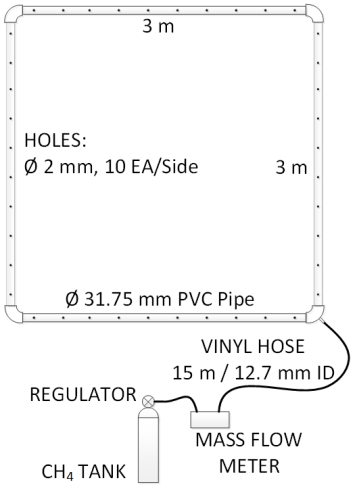

Figure B1. PVC disseminator assembly for producing diffuse gas releases with release setup. Point releases were produced directly from the vinyl hose without the PVC structure.

Appendix C: Controlled release results

Tables C1 and C2 contain results from the blind controlled release testing and related definitions for interpretation.

Table C1. Definitions of columns in summary of results in Table C2

Parameter	Parameter Description
relID	first number is release location designator; second number is sequential release number at that location
det	binary value of a detection during the release (1 = detected, 0 = not detected)
relScan	number of sensor scans completed during release period
detScan	number of sensor scans resulting in detection during release period
relBox	grid box where release was conducted
emisBox	box identified by analytics as the emission location
locPrec	UNIT: emisBox equal to relBox; GROUP: emisBox adjacent to relBox; FACIL: emisBox not equal or adjacent to relBox
relRate	metered release rate in grams per hour (g h^{-1})
emisRate	estimated emissions rate in grams per hour (g h^{-1})
quantAccAbs	emisRate minus relRate in grams per hour (g h^{-1})
quantAccRel	quantAccAbs divided by relRate
detTime	time between a detection and the last data point needed to establish that detection (HH:MM:SS)
windSpdAvg	average observed wind speed during release period, included for context

Table C2. Results for all blind releases

relID[a]	det	relScan	detScan	relBox	emisBox[b]	locPrec	relRate	emisRate[b]	quantAccAbs	quantAccRel	detTime	windSpAvg
05-01	1	8	1	1-3	5-1	FACIL	215.1	72	−143.1	−0.665	08:41:21	1.9
05-02	1	4	3	1-3	1-4	GROUP	1290.6	4680	3389.4	2.626	07:23:00	3.6
05-03	0	7	0	1-3	X-X	N/A	430.2	0	−430.2	−1	00:00:00	5.1
06-01	1	4	2	2-2	3-1	GROUP	860.4	576	−284.4	−0.331	03:58:50	5.0
06-02	1	3	2	2-2	2-2	UNIT	2151	1404	−747	−0.347	03:20:24	4.5
06-03	1	4	3	2-2	3-5	FACIL	860.4	2160	1299.6	1.51	02:31:33	4.7
07-01	1	3	2	4-5	4-5	UNIT	2151	1152	−999	−0.464	09:02:58	2.7
07-02	1	3	3	4-5	4-5	UNIT	1720.8	1728	7.2	0.004	08:28:24	2.9
07-03	0	7	0	4-5	X-X	N/A	215.1	0	−215.1	−1	00:00:00	3.3
08-01	1	4	3	4-1	5-2	GROUP	860.4	1440	579.6	0.674	06:47:26	3.1
08-02	1	8	2	4-1	4-1	UNIT	430.2	576	145.8	0.339	05:09:42	4.1
08-03	1	4	4	4-1	5-2	GROUP	1075.5	2484	1408.5	1.31	04:14:53	3.2
09-01	1	8	5	1-1	1-1	UNIT	860.4	504	−356.4	−0.414	09:50:00	3.8
09-02	0	5	0	1-1	X-X	N/A	322.65	0	−322.7	−1	00:00:00	5.0
10-01	0	7	0	4-3	X-X	N/A	322.65	0	−322.7	−1	00:00:00	4.4
10-02	1	3	2	4-3	4-2	GROUP	2151	972	−1179	−0.548	05:49:00	4.4
10-03	1	4	1	4-3	5-1	FACIL	645.3	540	−105.3	−0.163	05:10:10	4.0
10-04	1	5	4	4-3	4-3	UNIT	1075.5	648	−427.5	−0.397	04:07:52	3.7
11-01	0	3	0	2-4	X-X	N/A	172.08	0	−172.1	−1	00:00:00	2.7
11-02	1	5	1	2-4	1-4	GROUP	645.3	72	−573.3	−0.888	09:10:41	3.5
11-03	0	4	0	2-4	X-X	N/A	430.2	0	−430.2	−1	00:00:00	3.3
12-01	1	8	3	3-3	3-4	GROUP	344.16	468	123.8	0.36	07:45:44	3.8
12-02	1	6	3	3-3	3-3	UNIT	989.46	1008	18.5	0.019	06:56:15	3.8
13-01	0	7	0	2-1	X-X	N/A	430.2	0	−430.2	−1	00:00:00	3.7
13-02	1	7	1	2-1	4-5	FACIL	645.3	1080	434.7	0.674	04:28:55	3.4
13-03	1	5	1	2-1	5-5	FACIL	817.38	288	−529.4	−0.648	03:40:15	4.0
14-01	1	5	4	5-5	5-5	UNIT	774.36	792	17.6	0.023	10:35:26	2.2
14-02	1	7	1	5-5	5-5	UNIT	645.3	360	−285.3	−0.442	09:30:06	3.9
15-01	0	15	0	3-3	X-X	N/A	172.08	0	−172.1	−1	00:00:00	3.2
15-02	0	6	0	3-3	X-X	N/A	322.65	0	−322.7	−1	00:00:00	4.1
15-03	0	8	0	3-3	X-X	N/A	559.26	0	−559.3	−1	00:00:00	3.5
15-04	1	5	3	3-3	5-5	FACIL	1075.5	1008	−67.5	−0.063	11:03:50	3.9
15-05	0	4	0	3-3	X-X	N/A	215.1	0	−215.1	−1	00:00:00	4.5
15-06	0	4	0	3-3	X-X	N/A	430.2	0	−430.2	−1	00:00:00	4.7
15-07	1	6	3	3-3	4-4	GROUP	1505.7	1476	−29.7	−0.02	08:27:57	4.6
15-08	0	7	0	3-3	X-X	N/A	430.2	0	−430.2	−1	00:00:00	4.0
15-09	0	7	0	3-3	X-X	N/A	645.3	0	v645.3	−1	00:00:00	5.0
16-01	0	6	0	1-1	X-X	N/A	430.2	0	−430.2	−1	00:00:00	5.3
16-02	1	4	3	1-1	1-4	FACIL	860.4	1872	1011.6	1.176	04:21:17	4.4
16-03	1	4	2	1-1	2-1	GROUP	2151	972	−1179	−0.548	03:38:09	5.6
16-04	0	4	0	1-1	X-X	N/A	430.2	0	−430.2	−1	00:00:00	4.6
16-05	0	4	0	1-1	X-X	N/A	1505.7	0	−1505.7	−1	00:00:00	5.6

a Releases with releaseID values beginning with digits less than 05 were unblind releases and are not presented in these results.

b Emission rate and location information are only present in the table for those releases which were positively detected.

Appendix D: Detection of off-site emissions sources

On the morning of 17 March 2022, there were 105 detections in a span of about 80 minutes during which time no controlled releases were conducted. A nearby Picarro G2301 sampling ambient air located slightly south of the southern edge of the monitored area showed an elevated background CH_4 volume mixing ratio. Figure D1 shows the GreenLITE™ detections and the volume mixing ratio measured by the Picarro.

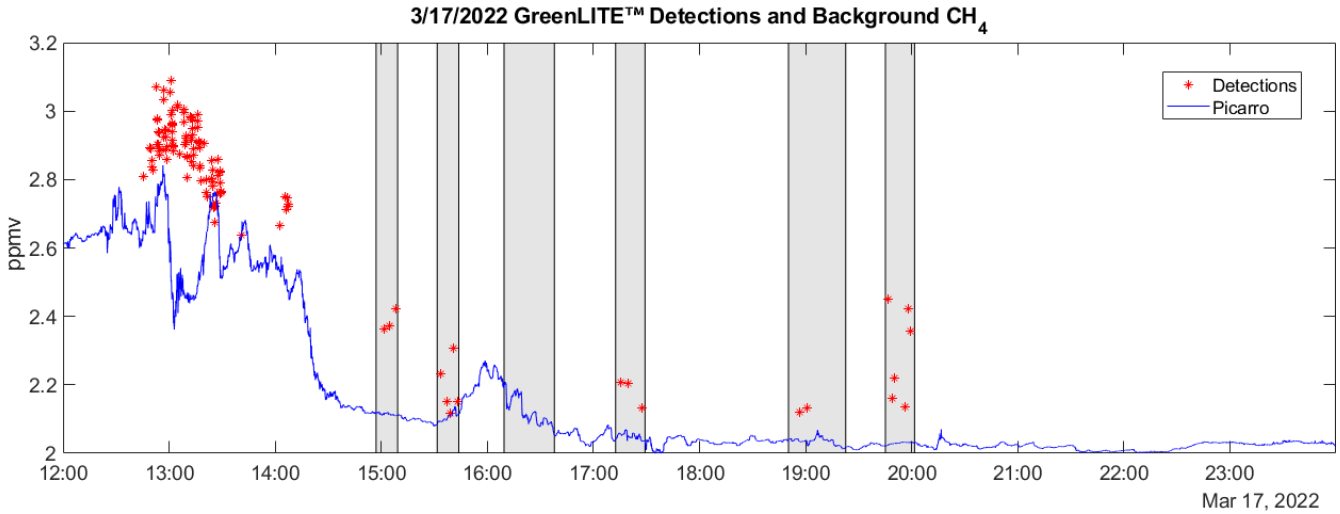

Figure D1. Detection results showing evidence of large offsite methane source. A large cluster of GreenLITE™ detections (red stars) coincides with elevated background volume mixing ratio measured by a nearby Picarro G2301 (blue line, location indicated by black star near bottom of Figure D2) on 17 March 2022. Gray shaded regions represent controlled release periods.

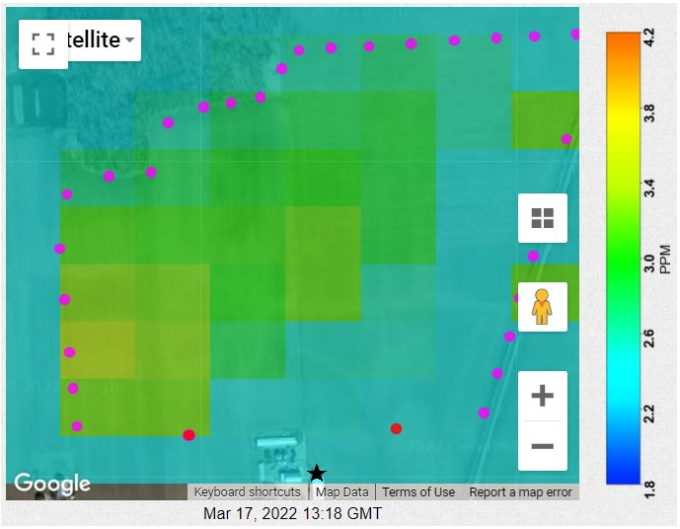

Figure D2. 2-D reconstruction of CH_4 emissions during period of frequently occurring detections. Evidence of an offsite source southwest of the monitored area is visible. Wind direction at this time was from the southwest at 218°. Red circles are the two transceiver locations along the southern edge, magenta circles are the reflector locations around the perimeter of the testing area, and the black star near the bottom indicates the location of the Picarro ambient CH_4 sensor. Map Source: Google Maps © 2022

The 2-D reconstruction of the mixing ratio as measured by GreenLITE™ and shown in Figure D2 indicates an offsite source blowing into the monitored area. The wind direction during the time period in which the cluster of non-controlled-release detections occurred ranged from 210 to 240 degrees (south-southwest to southwest). A very similar event occurred on March 21, with 93 detections occurring in 104 minutes. Because the detections in these time periods were caused by an outside source, and because the CMP states that detections identified as "OFF_FACILITY" are not classified as FP detections, they have not been counted as FP detections in these metrics or included in the calculation of FPF.

Appendix E: Detection time results

Figure E1 shows the Detection Time as a function of release rate. As expected, Detection Time trends toward shorter times as release rates increase. At the time the test plan was audited by the METEC representative, the real-time detection algorithm was not fully implemented. In following the audited test plan, Detection Time results reported to EPA were generated with data analyzed for detections at the end of each test day and ranged from 6 hours, 19 minutes to 11 hours, 4 minutes (equal to the elapsed time from the chord measurement indicating a detection to the end of the daily collection period).

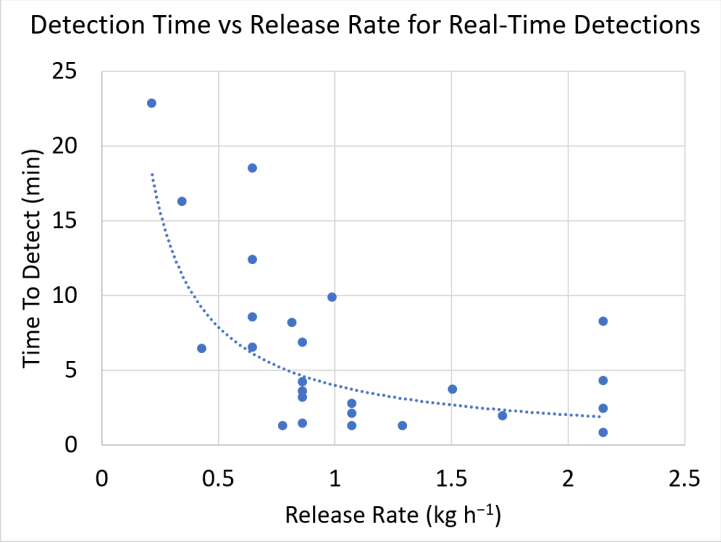

Figure E1. Detection times as a function of release rate using real-time detection algorithm. Detection times appear to follow a power fit in relation to gas release rate.

References

Alden, CB, Coburn, SC, Wright, RJ, Baumann, E, Cossel, K, Perez, E, Hoenig, E, Prasad, K, Coddington, I, Rieker, GB. 2019. Single-blind quantification of natural gas leaks from 1 km distance using frequency combs. *Environmental Science & Technology* **53**(3): 2908–17. DOI: https://doi.org/10.1021/acs.est.8b06259.

Bell, C, Ilonze, C, Duggan, A, Zimmerle, D. 2023. Performance of continuous emission monitoring solutions under single-blind controlled testing protocol. *Environmental Science & Technology* **57**(14): 5794–5805. DOI: https://doi.org/10.1021/acs.est.2c09235.

Bell, C, Rutherford, J, Brandt, A, Sherwin, E, Vaughn, T, Zimmerle, D. 2022. Single-blind determination of methane detection limits and quantification accuracy using aircraft-based LiDAR. *Elementa: Science of the Anthropocene* **10**(1): 00080. DOI: https://doi.org/10.1525/elementa.2022.00080.

Blakley, C, Carman, C, Korose, C, Luman, D, Zimmerman, J, Frish, M, Dobler, J, Blume, N, Zaccheo, S. 2020. Application of emerging monitoring techniques at the Illinois Basin – Decatur Project. *International Journal of Greenhouse Gas Control* **103**: 103188. DOI: https://doi.org/10.1016/j.ijggc.2020.103188.

Chowdhury, B, Karamchandani, PK, Sykes, RI, Henn, DS, Knipping, E. 2015. Reactive puff model SCICHEM: Model enhancements and performance studies. *Atmospheric Environment* **117**: 242–258. DOI: https://doi.org/10.1016/j.atmosenv.2015.07.012.

Colorado State University (CSU) Energy Institute. Advancing Development of Emissions Detection. https://energy.colostate.edu/metec/aded, last access: 25 Mar 2024.

Dobler, JT, Zaccheo, TS, Blume, N, Braun, M, Botos, C, Pernini, TG. 2015. Spatial mapping of greenhouse gases using laser absorption spectrometers at local scales of interest. Proceedings of SPIE **9645**: Lidar Technologies, Techniques, and Measurements for Atmospheric Remote Sensing XI, 96450K. Toulouse, France. DOI: https://doi.org/10.1117/12.2197713.

Dobler, JT, Zaccheo, TS, Pernini, TG, Blume, N, Broquet, G, Vogel, F, Ramonet, M, Braun, M, Staufer, J, Ciais, P, Botos, C. 2017. Demonstration of spatial greenhouse gas mapping using laser absorption spectrometers on local scales. *Journal of Applied Remote Sensing* **11**(1): 014002. DOI: https://doi.org/10.1117/1.JRS.11.014002.

International Energy Agency (IEA), Methane Tracker 2021. https://www.iea.org/reports/methane-tracker-2021/methane-and-climate-change, last access:25 Mar 2024.

Johnson, D, Clark, N, Heltzel, R, Darzi, M, Footer, TL, Herndon, S, Thoma, ED. 2022. Methane emissions from oil and gas production sites and their storage tanks in West Virginia. *Atmospheric Environment: X* **16**: 100193. DOI: https://doi.org/10.1016/j.aeaoa.2022.100193.

Lian, J, Bréon, FM, Broquet, G, Zaccheo, TS, Dobler, J, Ramonet, M, Staufer, J, Santaren, D, Xueref-Remy, I, Ciais, P. 2019. Analysis of temporal and spatial variability of atmospheric CO2 concentration within Paris from the GreenLITE™ laser imaging experiment. *Atmospheric Chemistry and Physics* **19**: 13809–13825. DOI: https://doi.org/10.5194/acp-19-13809-2019.

Lyon, DR, Alvarez, RA, Zavala-Araiza, D, Brandt, AR, Jackson, RB, Hamburg, SP. 2016. Aerial surveys of elevated hydrocarbon emissions from oil and gas production sites. *Environmental Science & Technology* **50**(9): 4877–4886. DOI: https://doi.org/10.1021/acs.est.6b00705.

Lyon, DR, Zavala-Araiza, D, Alvarez, RA, Harriss, R, Palacios, V, Lan, X, Talbot, R, Lavoie, T, Shepson, P, Yacovitch, TI, Herndon, SC. 2015. Constructing a spatially resolved methane emission inventory for the Barnett Shale region. *Environmental Science & Technology* **49**(13): 8147–8157. DOI: https://doi.org/10.1021/es506359c.

Nathan, BJ, Golston, LM, O'Brien, AS, Ross, K, Harrison, WA, Tao, L, Lary, DJ, Johnson, DR, Covington, AN, Clark, NN, Zondlo, MA. 2015. Near-field characterization of methane emission variability from a compressor station using a model aircraft. *Environmental Science & Technology* **49**(13): 7896–7903. DOI: https://doi.org/10.1021/acs.est.5b00705.

National Academies of Sciences, Engineering, and Medicine. 2018. Improving characterization of anthropogenic methane emissions in the United States. *The National Academies Press*, Washington, DC. DOI: https://doi.org/10.17226/24987.

Pernini, TG, Zaccheo, TS, Dobler, J, Blume, N. 2022. Estimating oil sands emissions using horizontal path-integrated column measurements. *Atmospheric Measurement Techniques* **15**: 225–240. DOI: https://doi.org/10.5194/amt-15-225-2022.

Riddick, SN, Ancona, R, Mbua, M, Bell, CS, Duggan, A, Vaughn, TL, Bennett, K, Zimmerle, DJ. 2022. A quantitative comparison of methods used to measure smaller methane emissions typically observed from superannuated oil and gas infrastructure. *Atmospheric Measurement Techniques* **15**(21): 6285–6296. DOI: https://doi.org/10.5194/amt-2022-9.

Sherwin, ED, Chen, Y, Ravikumar, AP, Brandt, AR. 2021. Single-blind test of airplane-based hyperspectral methane detection via controlled releases. *Elementa: Science of the Anthropocene* **9**(1). DOI: https://doi.org/10.1525/elementa.2021.00063.

United States Environmental Protection Agency (EPA). Overview of greenhouse gases. https://www.epa.gov/ghgemissions/overview-greenhouse-gases, last access: 6 June 2023.

United States Environmental Protection Agency (EPA). Understanding global warming potentials. https://www.epa.gov/ghgemissions/understanding-global-warming-potentials, last access: 6 June 2023.

Vaughn, TL, Bell, CS, Pickering, CK, Schwietzke, S, Heath, GA, Pétron, G, Zimmerle, DJ, Schnell, RC, Nummedal, D. 2018. Temporal variability largely explains top-down/bottom-up difference in methane emission estimates from a natural gas production region. *Proceedings of the National Academy of Sciences USA* **115**(46): 11712–11717. DOI: https://doi.org/10.1073/pnas.1805687115.

Watremez, X, Marble, A, Baron, T, Marcarian, X, Dubucq, D, Donnat, L, Cazes, L, Foucher, PY, Dano, R, Elie, D, Chamberland, M, Gagnon, JP, Gay, LB, Dobler, J, Ostrem, R, Russu, A, Schmidt, M, Zaouak, O. 2018. Remote sensing technologies for detecting, visualizing and quantifying gas leaks. *Society of Petroleum Engineers International Conference and Exhibition on Health, Safety, Security, Environment, and Social Responsibility.* Abu Dhabi, UAE. DOI: https://doi.org/10.2118/190496-MS.

Zaccheo, TS, Blume, N, Pernini, T, Dobler, J, Lian, J. 2019. Bias correction of long-path CO2 observations in a complex urban environment for carbon cycle model inter-comparison and data assimilation. *Atmospheric Measurement Techniques* **12**: 5791–5800. DOI: https://doi.org/10.5194/amt-12-5791-2019.

Zavala-Araiza, D, Lyon, DR, Alvarez, RA, Davis, KJ, Harriss, R, Herndon, SC, Karion, A, Kort, EA, Lamb, BK, Lan, X, Marchese, AJ, Pacala, SW, Robinson, AL, Shepson, PB, Sweeney, C, Talbot, R, Townsend-Small, A,

Yacovitch, TI, Zimmerle, DJ, Hamburg, SP. 2015. Reconciling divergent estimates of oil and gas methane emissions, *Proceedings of the National Academy of Sciences USA* **112**(51): 15597–15602. DOI: https://doi.org/10.1073/pnas.1522126112.

Zimmerle, D. 2020. METEC Controlled Test Protocol: Continuous monitoring emission detection and quantification. *Colorado State University Energy Institute*. Revision 1.0. DOI: https://doi.org/10.25675/10217/235364.

Author contributions

Contributed to conception and design: JTD, NB, CB

Contributed to acquisition of data: JTD, DM

Contributed to analysis and interpretation of data: NB, TGP, TSZ, CB

Drafted and/or revised the article: NB, TGP, JTD, TSZ, DM, CB

Approved the submitted version for publication: NB, TGP, JTD, TSZ, DM, CB

Acknowledgement

The authors acknowledge Michael Braun for his assistance in designing and constructing the gas dissemination system used in this study.

Funding

This work was supported by the United States Environmental Protection Agency SBIR Program under grant number 68HERC22C0013.

Competing interests

The GreenLITE™ system has been co-developed by Spectral Sensor Solutions, LLC (S3) and Atmospheric and Environmental Research, Inc (AER). NB, JTD, and DM are employees of S3. TGP and TSZ are employees of AER.

‡ Subsequent to the work described in this manuscript, Clay Bell began working for bpx energy, headquartered in Denver, Colorado. bpx energy did not participate in the drafting of this paper and the views set forth in the paper do not necessarily reflect those of bpx energy.

Data accessibility

Sample data sets and results corresponding to this study are available upon request from the corresponding author.